Letter

Chiral excitations and the intermediate-field regime in the Kitaev magnet $\alpha - RuCl_3$

Anuja Sahasrabudhe,[1,*] Mikhail A. Prosnikov,[2] Thomas C. Koethe,[1] Philipp Stein,[1] Vladimir Tsurkan,[3,4] Alois Loidl,[3] Markus Grüninger,[1] Hamoon Hedayat,[1,†] and Paul H. M. van Loosdrecht[1,‡]

[1]*Institute of Physics II, University of Cologne, 50937 Cologne, Germany*

[2]*High Field Magnet Laboratory (HFML-EMFL), Radboud University, 6525 ED Nijmegen, The Netherlands*

[3]*University of Augsburg, 86159 Augsburg, Germany*

[4]*Institute of Applied Physics, MD 2028, Chisinau, Republic of Moldova*

(Received 4 May 2023; accepted 18 January 2024; published 5 April 2024)

In the Kitaev magnet α-$RuCl_3$, the existence of a magnetic-field-induced quantum spin-liquid phase and of anyonic excitations is controversially discussed. We address this elusive, exotic phase via helicity-dependent Raman scattering and analyze the Raman optical activity of excitations as a function of magnetic field and temperature. The hotly debated field regime between 7.5 and 10.5 T is characterized by clear spectroscopic signatures such as a plateau of the Raman optical activity of the dominant, chiral spin-flip excitation. This provides direct evidence for the existence of a distinct intermediate-field regime with an intriguing ground state featuring chiral excitations.

DOI: 10.1103/PhysRevResearch.6.L022005

More than a decade ago, Kitaev proposed an exactly solvable model for a spin-$\frac{1}{2}$ system on a honeycomb lattice with bond-directional nearest-neighbor exchange couplings that hosts a quantum spin-liquid (QSL) ground state [1]. The collective excitations above this ground state are gapless Majorana fermions and visons. In the presence of an external magnetic field, the Majorana fermions are gapped. The gapped spectrum hosts a chiral Majorana mode responsible for thermal edge transport and the emergent excitations are non-Abelian anyons [1].

Strong experimental efforts have been triggered by the possibility to achieve dominant Kitaev exchange and the related exotic excitations in real materials [2]. In this context, α-$RuCl_3$ has been touted as a potential candidate that could possess a QSL phase [3–8], which in turn has sparked a flurry of research in exploring its physical properties [9–13]. Unlike an ideal QSL that remains disordered even at vanishing temperature, the presence of additional exchange interactions in α-$RuCl_3$ yields antiferromagnetic zigzag (ZZ) order below 7 K and for external magnetic fields below 7 T [9–11,14]. For strong enough magnetic fields, a field-induced spin-polarized phase is observed [15–17]. It is still possible though that between these high- and low-field phases, bond-directional interactions take over in an intermediate-field regime (IFR), thereby preparing a conducive ground for the appearance of a QSL.

In this purported intermediate-field regime, thermal conductivity measurements [18–20] have displayed a direct signature of a chiral Majorana edge mode (and hence of a QSL)—viz., a half-integer quantized plateau in the transverse heat conductivity [21–23]. However, half-integer quantization of the thermal conductivity and, consequently, the role of Majorana fermions as heat carriers has been challenged [24–26]. Meanwhile, thermodynamic experiments such as thermal expansion, magnetostriction, and the magnetocaloric effect provide conflicting conclusions about the presence of the QSL phase in the field regime of 7.5(5) T to 11 T for a field applied parallel to the honeycomb plane [12,27–29]. Recent evidence in favor of the QSL phase comes from the observation of oscillations of the thermal conductivity in this field regime [25].

When studied using spectroscopic experiments, α-$RuCl_3$ shows a low-energy multiparticle continuum proposed to be of Majorana fermions [5,6,30]. Curiously, this continuum is already present in the magnetically ordered phase in zero field. Upon suppression of the antiferromagnetic ZZ phase in a large external magnetic field, the continuum acquires a gap and the spectrum exhibits a sharp excitation that is smoothly connected to a spin-flip excitation in the field-polarized limit [15]. Altogether, the spectroscopic data reported thus far do not provide any signature of a distinct IFR [8,15–17,31]. In Raman scattering at 2 K in a magnetic field, Wulferding *et al.* [32] observed an excitation which they interpreted as a Majorana bound state. However, the field was tilted by 18° out of the honeycomb plane and the measurements were restricted to 10 T. Hence the data could not capture any possible difference between the high-field and the intermediate-field regimes. Remarkably, this excitation has not been observed in another Raman

*sahasrabudhe@ph2.uni-koeln.de
†hedayat@ph2.uni-koeln.de
‡pvl@ph2.uni-koeln.de

Published by the American Physical Society under the terms of the Creative Commons Attribution 4.0 International license. Further distribution of this work must maintain attribution to the author(s) and the published article's title, journal citation, and DOI.

scattering study of α-$RuCl_3$ in high-magnetic fields [15], thus obstructing the clarity of opinion about the presence of an IFR.

Raman scattering is expected to be an effective probe for emergent Majorana fermions [6,33,34] and anyonic excitations. Experiments performed by Pinczuk *et al.* have already demonstrated the strength of Raman scattering in probing the emergent anyonic excitations of the fractional quantum Hall effect [35–37]. Recently, it has been suggested that these anyonic excitations are chiral and may show fingerprints in helicity-dependent Raman scattering [38,39]. Inspired by these ideas, we performed helicity-dependent Raman scattering on α-$RuCl_3$. The blueprint for this is to compare the Raman intensities for circularly polarized light [40] in the four different polarization geometries $I_{++}, I_{--}, I_{+-}, I_{-+}$, where the first (second) index denotes the circular polarization of the incident (scattered) light. As the continuum and the magnetic excitations in α-$RuCl_3$ do not scatter in I_{++} and I_{--} (see the Supplemental Material [41]), we focus on the Raman optical activity (ROA) defined as

$$\mathrm{ROA} = \frac{I_{+-} - I_{-+}}{I_{+-} + I_{-+}}. \tag{1}$$

ROA is a detectable quantity that is intimately connected with the chirality of excitations [40,42,43]. Chiral excitations possess handedness and are asymmetric under inversion. For example, let us consider magnons. Magnons in a ferromagnet are chiral and are right circularly polarized with respect to the direction of magnetization [44], while antiferromagnets have two degenerate magnon branches with opposite chirality. In the particular case of a ferromagnet, only one of the two incident polarizations σ^+ and σ^- yields a Raman signal and this shows ROA $= 1$ [45–47]. In antiferromagnets, an external magnetic field can lift the degeneracy of magnons, which can again be detected using ROA [48].

In this Letter, we focus on exploring the chirality of magnetic excitations in α-$RuCl_3$ through the associated ROA. For an external magnetic field B large enough to suppress the ZZ phase, we will show three different trends in ROA. These will be pinpointed as characteristic fingerprints of three distinct field-induced magnetic regimes. One stunning example is the observation of a plateau of ROA $= 1$ of the dominant magnetic excitation in the field range of 7.5 T to 10.5 T which serves as a spectroscopic signature of a prominent intermediate-field regime.

For these experiments, high-quality single crystals of α-$RuCl_3$ were prepared by the vacuum sublimation method [7]. A monoclinic $C2/m$ structure is confirmed using polarized Raman spectroscopy (see the Supplemental Material [41]). The sample is placed in a cryostat and cooled down to 1.7 K. The magnetic field is applied within the *ab* plane, perpendicular to a Ru-Ru bond. The light polarization is defined with respect to the z axis. Left (right) circular light is represented as σ^+ (σ^-) as it projects spin angular momentum $+\hbar$ ($-\hbar$) onto the quantization axis. The experimental geometry is defined using the Porto notation as $z(\sigma^+\sigma^-)\bar{z}$ and $z(\sigma^-\sigma^+)\bar{z}$; see Figs. 1(a), 1(b) and the Supplemental Material [41] for details. We refer to the corresponding Raman intensities as I_{+-} and I_{-+}, respectively. The data have been normalized in the range of the higher-energy phonons from 27 to 43 meV.

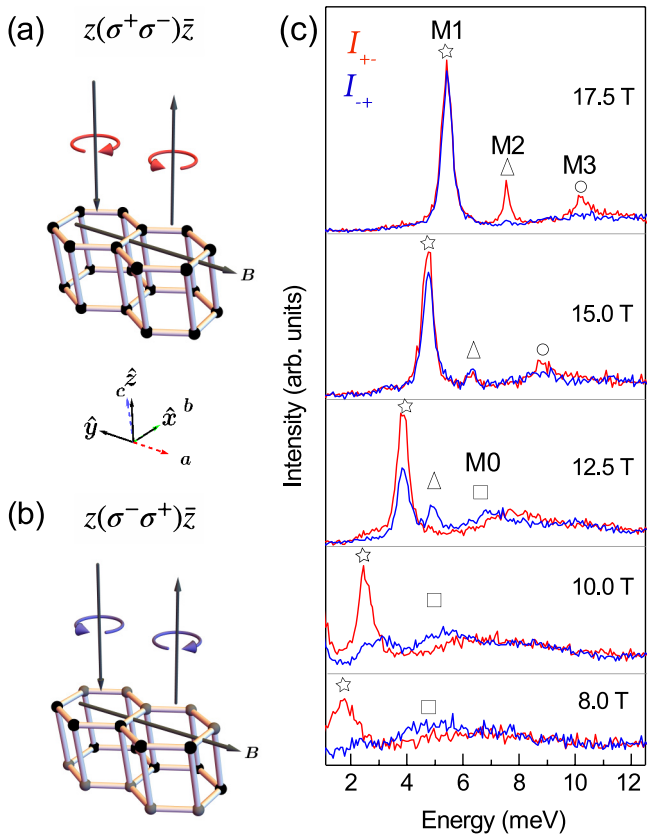

FIG. 1. Schematic of experimental geometry for measuring the helicity-resolved Raman intensities (a) I_{+-} and (b) I_{-+} as plotted in (c) for different magnetic-field strengths. Square, star, triangle, and circle symbols denote the magnetic excitations M0, M1, M2, and M3, respectively.

Figure 1(c) shows the helicity-dependent Raman response for $B > B_c$ (=7.5 T). Overall, the observed features agree with previous Raman results [15,32]. The data show the magnetic modes M0, M1, M2, and M3, and a broad magnetic multiparticle continuum. The M0 peak has been observed by Wulferding *et al.* [32,49] in a tilted magnetic field up to 10 T with incident σ^- polarization. They attributed this feature to a singlet Majorana bound state as its excitation energy remained insensitive to the magnetic field. The M1 mode has been identified as a spin-flip excitation with $|\Delta S| = 1$ in the fully spin-polarized limit, i.e., for infinite magnetic field, while M2 has been attributed to a two-particle bound state [15,32]. The feature M3 has been interpreted either as a two-particle excitation since its energy at high fields equals roughly twice the energy of M1 [15] or as a three-particle bound state [32]. We emphasize that this picture applies to the high-field limit [15,16,32].

From the helicity dependence, it is immediately clear that the magnetic features M0, M1, M2, and M3 exhibit chirality. The effect of the magnetic field on the chirality of these excitations allows us to distinguish different regimes. To this end, Fig. 2(a) depicts the ROA on a color scale. We first focus on the ROA of M1, which can be continuously traced down to B_c.

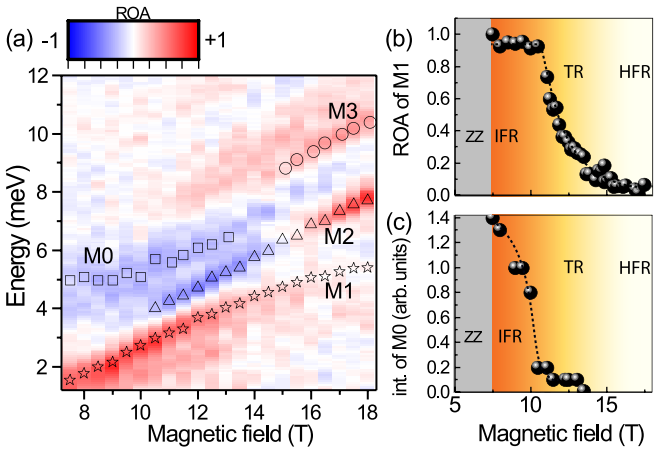

FIG. 2. (a) ROA as a function of energy and field. Symbols denote the peak energies of M0, M1, M2, and M3. (b) ROA of the M1 mode. The different trends in the ROA of M1 can be used to determine the three distinct magnetic-field regimes. Orange region: IFR with ROA = 1; color gradient: transition regime (TR); white region: high-field regime (HFR) with ROA ≈ 0. The gray-shaded region indicates the ordered ZZ phase. Dashed lines: guide to the eye. (c) Integrated intensity of the M0 mode as a function of magnetic field. In all three panels, error bars are smaller than or equal to the symbol size.

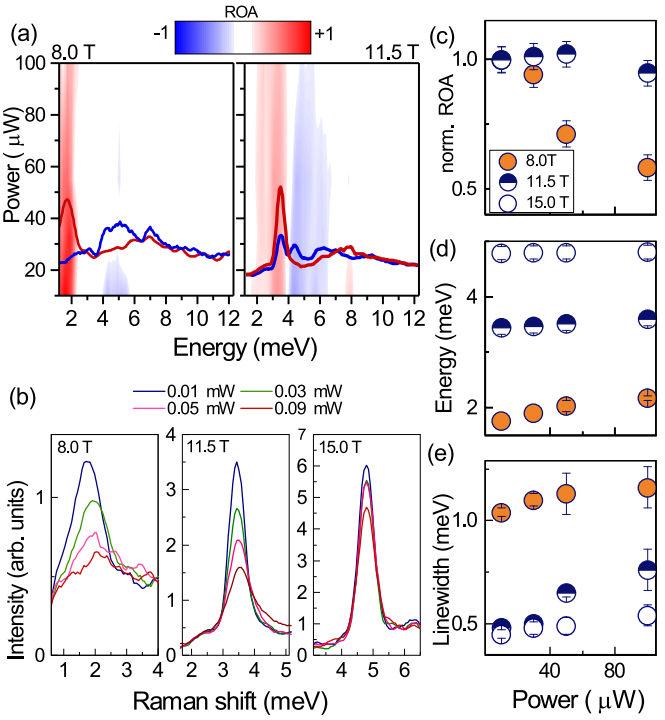

FIG. 3. (a) Power dependence of ROA at 8 and 11.5 T. Red (blue) areas represent larger scattering in I_{+-} (I_{-+}). As a reference, the red and blue solid lines show I_{+-} and I_{-+} at 10 μW. At 8 T, the M1 mode in the I_{+-} channel shows maximum power sensitivity around 40 μW ($T \sim 7$ K), while M0 in the I_{-+} channel disappears around 20 μW ($T < 7$ K). (b) Effect of laser power on M1 in I_{+-} in different field regimes. (c) Power-induced change in ROA of M1 at 8 and 11.5 T. (d),(e) Power dependence of energy and linewidth of the M1 mode in the I_{+-} channel.

Values for ROA are obtained via Eq. (1), using the integrated intensities obtained by fitting a Lorentzian to the M1 mode in I_{+-} and I_{-+} (see the Supplemental Material [41]). The result is depicted in Fig. 2(b), which reveals three distinct trends in the ROA of M1. We find a clear plateau with ROA ≈ 1 from 7.5 T to 10.5 T in the IFR, a continuous decrease in ROA in the transition regime from 10.5 T to 15 T, and ROA ≈ 0 in the high-field regime above 15 T.

Supporting evidence for the thus identified onset of the high-field regime at 15 T emanates from the behavior of M0, M2, and M3; see Fig. 2(a). The ROA of M2 crosses zero around 15 T and undergoes a drastic change from ROA = −1 at 10.5 T to ROA = +1 at 18 T. Concerning M3, a clear peak is only identified above 15 T, while a consistent broad feature with ROA > 0 is visible from 10.5 T [see Figs. 1(c) and 2(a)]. In contrast, M0 is only detected below 15 T, where it shows a negative ROA [cf. Figs. 1(c) and 2(c)]. As we do not observe any pronounced changes in ROA of these features from 15 to 30 T (see the Supplemental Material [41]), we identify $B \sim 15$ T as the onset of the high-field regime.

Having identified the high-field regime, we now discuss the observations of the IFR. Apart from a fully chiral M1, the only other chiral excitation that is observed in this regime is M0. The energy (open squares) and the integrated intensity of the M0 mode are plotted in Figs. 2(a) and 2(c), respectively. From 7.5 to 10.5 T, the energy of M0 remains constant, while the intensity shows a pronounced decrease. Above 10.5 T, M2 starts to peak in the energy window of M0, requiring two Lorentzians to account for the presence of both peaks. Simultaneously, the excitation energy of M0 starts to increase linearly with B with almost the same slope as M2. In summary, all relevant excitations (M0, M1, and M2) show distinct changes at 10.5T, providing clear spectroscopic evidence for the existence of an IFR.

After identifying the magnetic-field range of the IFR in our Raman data, we turn to the sensitivity of this phase to temperature, focusing on the properties of the chiral excitations M0 and M1. The temperature dependence is examined by varying the power of the incident light so as to avoid a mechanical drift of the sample. We estimate that 40 and 100 μW correspond to 7 and 13 K, respectively [50]. Figure 3(a) exemplifies the power-dependent change of ROA at 8 and 11.5 T, i.e., inside and just above the IFR, respectively. For ease of visualization, we have superimposed smoothened reference spectra taken at 10 μW. At 8 T, the spectra show M1 and M0 around 1.5 and 5 meV, respectively; cf. Fig. 2(a). At 11.5 T, the peaks are shifted to around 3.2 and 6.0 meV while M2 appears around 4.5 meV. The color plot again pinpoints the opposite chiralities of M1 and M0. The power dependence reveals a further key difference between 8 and 11.5 T. In the IFR at 8 T, the chiralities of both M1 and M0 rapidly decline with increasing laser power, i.e., sample temperature. In contrast, the ROA of both modes is less sensitive to the laser power at 11.5 T. This is highlighted in Fig. 3(c), showing the normalized ROA of M1. At 40 μW (≈7 K), the ROA of M1 is suppressed by more than a factor of two at 8 T, but remains unaffected at 11.5 T.

Figure 3(b) shows the smoothened spectrum of M1 as observed in I_{+-}, while Figs. 3(d) and 3(e) show the energy and the linewidth of M1 as a function of power for different fields, obtained by fitting M1 in I_{+-} with a Lorentzian. The energy of M1 hardens with increasing laser power at 8 T. Again, this behavior is found to be unique to the IFR. Furthermore, the linewidth of M1 is much larger at 8 T than at higher fields.

Previous Raman scattering studies on α-$RuCl_3$ in high magnetic fields reported on I_{+-} [15] and I_{-+} [32]. Due to the chiral character of the magnetic excitations, in particular with M0 and M1 showing opposite chiralities, the key to a comprehensive picture of the magnetic Raman features and to a thorough understanding of the spectra lies in the comparison of the I_{+-} and I_{-+} channels, i.e., in the ROA. In particular, our ROA data measured over a wide range of magnetic fields above B_c allow us to unravel the distinct spectroscopic characteristics of the intermediate-field regime and to elucidate its properties.

The IFR is characterized by the presence of the two excitations M0 and M1, for which we find opposite chiralities. Furthermore, ROA = 1 for M1 within the IFR. To illustrate the importance of M0 and M1 being chiral, we consider the case of a simple paramagnet instead of a QSL above 7.5 T, where long-range zigzag order is suppressed by the magnetic field. The external magnetic field competes with exchange interactions. In this paramagnet scenario, it is feasible to neglect field-induced order at B_c and assume that the time average of the local magnetic moments tends to zero. In this case, the Raman tensor R of the excitations is defined by the crystallographic space group $C2/m$ [30]. The Raman intensity is given by $I_{is} = |e_s^\dagger R\, e_i|^2$, where e_s and e_i are the electric-field vectors of the scattered and the incident light. Since the crystallographic group is not chiral, we find $I_{+-} = I_{-+}$ and ROA = 0; see the Supplemental Material [41]. The pronounced ROA of the magnetic excitations M0 and M1 in the IFR indicates an unconventional ground state that is distinct from a conventional paramagnet.

Previously, M0 has been attributed to a singlet Majorana bound state [32]. While our results do not provide any direct evidence for a Majorana character, the large width of M0 speaks against a strict bound-state scenario, but rather suggests a resonance within the continuum close to its lower edge.

The mode M1 has been identified as a spin-flip excitation in the high-field regime [15]. Above 15 T, the ROA of M1 is negligible. The pronounced increase of the ROA with decreasing field and, in particular, the plateau with ROA = 1 in the IFR are clear signatures of a change of character of this mode. Remarkably, the plateau is observed in the range 7.5 T to 10.5 T, consistent with the intermediate-field regime where a QSL phase has been proposed to exist [12,18–20,25]. The linewidth γ of the M1 mode equals 0.5 meV in the high-field regime, where it corresponds to a spin flip; see Fig. 3(e). In the IFR, γ is enhanced by more than a factor of two. It is tempting to explain this increase of the linewidth in a scenario based on Majorana fermions, where the local spins decay into Majoranas and fluxes, giving rise to a substantial broadening of M1. However, at this point, the role of other scattering channels, for example, spin-phonon scattering, cannot be ruled out.

Lastly, we briefly comment on the nature of the M2 and M3 modes in the high-field phase. They both show a pronounced ROA, where the ROA of the M2 mode even changes sign at about 15 T. This observation is interesting in view of the prediction of the presence of topological magnons in the field-polarized phase of a Kitaev-Heisenberg magnet [51–53].

In conclusion, magnetic-field- and laser-power-dependent Raman optical activity experiments show the presence of distinct field-induced phases for α-$RuCl_3$. In particular, the upper limit of our identified intermediate-field regime is very close to the value of 11 T, above which the quantum oscillations intrinsic to a QSL phase vanish [25]. The intermediate-field regime shows intriguing spectroscopic features. The most salient features are a fully chiral response (ROA=1) of the strongest (M1) magnetic mode and the presence of a resonance mode (M0) on the lower edge of the magnetic Raman continuum which previously has been discussed in terms of a Majorana bound state [32]. The large width of both modes may suggest a fractional character of the fundamental magnetic excitations specific for the IFR, but at the same time speaks against a bound-state scenario. The laser-power dependence (i.e., temperature dependence) of the spectra indicates that the ground state in the IFR region is rather fragile as is demonstrated by the rapid decrease of the fully chiral response upon increasing temperature. In contrast, the ROA of the spectra in the high-field regime is hardly affected by the increased temperature. Though it is clear from the present and earlier experiments that the IFR has an unconventional ground state which could very well be a quantum spin-liquid state, its exact nature remains elusive at this point. The present work shows the power of ROA experiments in materials showing unconventional magnetism and sheds light on the intriguing chiral magnetic properties of the Kitaev-Heisenberg magnet α-$RuCl_3$, inspiring future research to realize a field-induced spin-liquid phase in α-$RuCl_3$ and other Kitaev-like systems.

We thank Aprem Joy, Ciarán Hickey, David Kaib, Roser Valenti, Daniel I. Khomskii, and Fulvio Parmigiani for insightful discussions. We thank Jonathan Buhot and Clément Faugeras for supporting preliminary experimental measurements. A.S. thanks Vivek Lohani for critical comments on the manuscript. M.A.P. thanks Matija Čulo and Peter C. M. Christianen for discussions and support during the experiment. The authors acknowledge financial support by the Deutsche Forschungsgemeinschaft (DFG, German Research Foundation) via Project No. 277146847 – CRC 1238 (Project B03), via Project No. 107745057 – TRR 180 (Project F5), and via Project No. VA117/15-1. A.L. and V.T. acknowledge financial support by the DFG through Grant No. TRR 80. V.T. acknowledges the financial support via the Project No. ANCD 20.80009.5007.19 (Moldova). This work was supported by HFML-RU/NWO-I, member of the European Magnetic Field Laboratory (EMFL).

[1] A. Kitaev, Anyons in an exactly solved model and beyond, Ann. Phys. **321**, 2 (2006).

[2] G. Jackeli and G. Khaliullin, Mott insulators in the strong spin-orbit coupling limit: From Heisenberg to a quantum

compass and Kitaev models, Phys. Rev. Lett. **102**, 017205 (2009).

[3] H.-S. Kim, V. V. Shankar, A. Catuneanu, and H.-Y. Kee, Kitaev magnetism in honeycomb α-$RuCl_3$with intermediate spin-orbit coupling, Phys. Rev. B **91**, 241110(R) (2015).

[4] A. Banerjee, J. Yan, J. Knolle, C. A. Bridges, M. B. Stone, M. D. Lumsden, D. G. Mandrus, D. A. Tennant, R. Moessner, and S. E. Nagler, Neutron scattering in the proximate quantum spin liquid α-$RuCl_3$, Science **356**, 1055 (2017).

[5] L. J. Sandilands, Y. Tian, K. W. Plumb, Y.-J. Kim, and K. S. Burch, Scattering continuum and possible fractionalized excitations in α-$RuCl_3$, Phys. Rev. Lett. **114**, 147201 (2015).

[6] J. Nasu, J. Knolle, D. L. Kovrizhin, Y. Motome, and R. Moessner, Fermionic response from fractionalization in an insulating two-dimensional magnet, Nat. Phys. **12**, 912 (2016).

[7] S.-H. Do, S.-Y. Park, J. Yoshitake, J. Nasu, Y. Motome, Y. S. Kwon, D. T. Adroja, D. J. Voneshen, K. Kim, T. H. Jang, J. H. Park, K.-Y. Choi, and S. Ji, Majorana fermions in the Kitaev quantum spin system α-$RuCl_3$, Nat. Phys. **13**, 1079 (2017).

[8] S.-H. Baek, S.-H. Do, K.-Y. Choi, Y. S. Kwon, A. U. B. Wolter, S. Nishimoto, J. Van Den Brink, and B. Büchner, Evidence for a field-induced quantum spin liquid in α-$RuCl_3$, Phys. Rev. Lett. **119**, 037201 (2017).

[9] R. D. Johnson, S. C. Williams, A. A. Haghighirad, J. Singleton, V. Zapf, P. Manuel, I. I. Mazin, Y. Li, H. O. Jeschke, R. Valentí, and R. Coldea, Monoclinic crystal structure of α-$RuCl_3$and the zigzag antiferromagnetic ground state, Phys. Rev. B **92**, 235119 (2015).

[10] H. B. Cao, A. Banerjee, J.-Q. Yan, C. A. Bridges, M. D. Lumsden, D. G. Mandrus, D. A. Tennant, B. C. Chakoumakos, and S. E. Nagler, Low-temperature crystal and magnetic structure of α-$RuCl_3$, Phys. Rev. B **93**, 134423 (2016).

[11] A. Banerjee, P. Lampen-Kelley, J. Knolle, C. Balz, A. A. Aczel, B. Winn, Y. Liu, D. Pajerowski, J. Yan, C. A. Bridges *et al.*, Excitations in the field-induced quantum spin liquid state of α-$RuCl_3$, npj Quantum Mater. **3**, 8 (2018).

[12] C. Balz, P. Lampen-Kelley, A. Banerjee, J. Yan, Z. Lu, X. Hu, S. M. Yadav, Y. Takano, Y. Liu, D. A. Tennant, M. D. Lumsden, D. Mandrus, and S. E. Nagler, Finite field regime for a quantum spin liquid in α-$RuCl_3$, Phys. Rev. B **100**, 060405(R) (2019).

[13] K. A. Modic, R. D. McDonald, J. Ruff, M. D. Bachmann, Y. Lai, J. C. Palmstrom, D. Graf, M. K. Chan, F. Balakirev, J. Betts *et al.*, Scale-invariant magnetic anisotropy in α-$RuCl_3$at high magnetic fields, Nat. Phys. **17**, 240 (2021).

[14] J. Wagner, A. Sahasrabudhe, R. B. Versteeg, L. Wysocki, Z. Wang, V. Tsurkan, A. Loidl, D. I. Khomskii, H. Hedayat, and P. H. van Loosdrecht, Magneto-optical study of metamagnetic transitions in the antiferromagnetic phase of α-$RuCl_3$, npj Quantum Mater. **7**, 28 (2022).

[15] A. Sahasrabudhe, D. Kaib, S. Reschke, R. German, T. Koethe, J. Buhot, D. Kamenskyi, C. Hickey, P. Becker, V. Tsurkan, A. Loidl, S. H. Do, K. Y. Choi, M. Gruninger, S. M. Winter, Z. Wang, R. Valenti, and P. H. M. van Loosdrecht, High-field quantum disordered state in α-$RuCl_3$: Spin flips, bound states, and multiparticle continuum, Phys. Rev. B **101**, 140410(R) (2020).

[16] A. N. Ponomaryov, L. Zviagina, J. Wosnitza, P. Lampen-Kelley, A. Banerjee, J.-Q. Yan, C. A. Bridges, D. G. Mandrus, S. E. Nagler, and S. A. Zvyagin, Nature of magnetic excitations in the high-field phase of α-$RuCl_3$, Phys. Rev. Lett. **125**, 037202 (2020).

[17] Z. Wang, S. Reschke, D. Hüvonen, S.-H. Do, K.-Y. Choi, M. Gensch, U. Nagel, T. Rõõm, and A. Loidl, Magnetic excitations and continuum of a possibly field-induced quantum spin liquid in α-$RuCl_3$, Phys. Rev. Lett. **119**, 227202 (2017).

[18] Y. Kasahara, T. Ohnishi, Y. Mizukami, O. Tanaka, S. Ma, K. Sugii, N. Kurita, H. Tanaka, J. Nasu, Y. Motome *et al.*, Majorana quantization and half-integer thermal quantum Hall effect in a Kitaev spin liquid, Nature (London) **559**, 227 (2018).

[19] T. Yokoi, S. Ma, Y. Kasahara, S. Kasahara, T. Shibauchi, N. Kurita, H. Tanaka, J. Nasu, Y. Motome, C. Hickey *et al.*, Half-integer quantized anomalous thermal Hall effect in the Kitaev material candidate α-$RuCl_3$, Science **373**, 568 (2021).

[20] M. Yamashita, J. Gouchi, Y. Uwatoko, N. Kurita, and H. Tanaka, Sample dependence of half-integer quantized thermal Hall effect in the Kitaev spin-liquid candidate α-$RuCl_3$, Phys. Rev. B **102**, 220404(R) (2020).

[21] J. Nasu, J. Yoshitake, and Y. Motome, Thermal transport in the Kitaev model, Phys. Rev. Lett. **119**, 127204 (2017).

[22] Y. Vinkler-Aviv and A. Rosch, Approximately quantized thermal Hall effect of chiral liquids coupled to phonons, Phys. Rev. X **8**, 031032 (2018).

[23] M. Ye, G. B. Halász, L. Savary, and L. Balents, Quantization of the thermal Hall conductivity at small Hall angles, Phys. Rev. Lett. **121**, 147201 (2018).

[24] E. Lefrançois, G. Grissonnanche, J. Baglo, P. Lampen-Kelley, J.-Q. Yan, C. Balz, D. Mandrus, S. E. Nagler, S. Kim, Y.-J. Kim, N. Doiron-Leyraud, and L. Taillefer, Evidence of a phonon Hall effect in the Kitaev spin liquid candidate α-$RuCl_3$, Phys. Rev. X **12**, 021025 (2022).

[25] P. Czajka, T. Gao, M. Hirschberger, P. Lampen-Kelley, A. Banerjee, J. Yan, D. G. Mandrus, S. E. Nagler, and N. P. Ong, Oscillations of the thermal conductivity in the spin-liquid state of α-$RuCl_3$, Nat. Phys. **17**, 915 (2021).

[26] J. A. N. Bruin, R. R. Claus, Y. Matsumoto, N. Kurita, H. Tanaka, and H. Takagi, Robustness of the thermal Hall effect close to half-quantization in α-$RuCl_3$, Nat. Phys. **18**, 401 (2022).

[27] S. Gass, P. M. Cônsoli, V. Kocsis, L. T. Corredor, P. Lampen-Kelley, D. G. Mandrus, S. E. Nagler, L. Janssen, M. Vojta, B. Büchner, and A. U. B. Wolter, Field-induced transitions in the Kitaev material α-$RuCl_3$probed by thermal expansion and magnetostriction, Phys. Rev. B **101**, 245158 (2020).

[28] S. Bachus, D. A. S. Kaib, Y. Tokiwa, A. Jesche, V. Tsurkan, A. Loidl, S. M. Winter, A. A. Tsirlin, R. Valentí, and P. Gegenwart, Thermodynamic perspective on field-induced behavior of α-$RuCl_3$, Phys. Rev. Lett. **125**, 097203 (2020).

[29] R. Schönemann, S. Imajo, F. Weickert, J. Yan, D. G. Mandrus, Y. Takano, E. L. Brosha, P. F. S. Rosa, S. E. Nagler, K. Kindo, and M. Jaime, Thermal and magnetoelastic properties of α-$RuCl_3$in the field-induced low-temperature states, Phys. Rev. B **102**, 214432 (2020).

[30] T. T. Mai, A. McCreary, P. Lampen-Kelley, N. Butch, J. R. Simpson, J.-Q. Yan, S. E. Nagler, D. Mandrus, A. R. Hight Walker, and R. V. Aguilar, Polarization-resolved Raman spectroscopy of α-$RuCl_3$and evidence of room-temperature two-dimensional magnetic scattering, Phys. Rev. B **100**, 134419 (2019).

[31] A. N. Ponomaryov, E. Schulze, J. Wosnitza, P. Lampen-Kelley, A. Banerjee, J.-Q. Yan, C. A. Bridges, D. G. Mandrus, S. E. Nagler, A. K. Kolezhuk, and S. A. Zvyagin, Unconventional spin dynamics in the honeycomb-lattice material α-$RuCl_3$:

High-field electron spin resonance studies, Phys. Rev. B **96**, 241107(R) (2017).

[32] D. Wulferding, Y. Choi, S.-H. Do, C. H. Lee, P. Lemmens, C. Faugeras, Y. Gallais, and K.-Y. Choi, Magnon bound states versus anyonic Majorana excitations in the Kitaev honeycomb magnet α-$RuCl_3$, Nat. Commun. **11**, 1603 (2020).

[33] J. Knolle, G.-W. Chern, D. L. Kovrizhin, R. Moessner, and N. B. Perkins, Raman scattering signatures of Kitaev spin liquids in A_2IrO_3 iridates with $a =$ Na or Li, Phys. Rev. Lett. **113**, 187201 (2014).

[34] J. Knolle, D. L. Kovrizhin, J. T. Chalker, and R. Moessner, Dynamics of fractionalization in quantum spin liquids, Phys. Rev. B **92**, 115127 (2015).

[35] A. Pinczuk, B. S. Dennis, L. N. Pfeiffer, and K. West, Observation of collective excitations in the fractional quantum Hall effect, Phys. Rev. Lett. **70**, 3983 (1993).

[36] M. Kang, A. Pinczuk, B. S. Dennis, L. N. Pfeiffer, and K. W. West, Observation of multiple magnetorotons in the fractional quantum Hall effect, Phys. Rev. Lett. **86**, 2637 (2001).

[37] A. R. Goñi, A. Pinczuk, J. S. Weiner, B. S. Dennis, L. N. Pfeiffer, and K. W. West, Observation of magnetoplasmons, rotons, and spin-flip excitations in GaAs quantum wires, Phys. Rev. Lett. **70**, 1151 (1993).

[38] D. X. Nguyen and D. T. Son, Probing the spin structure of the fractional quantum Hall magnetoroton with polarized Raman scattering, Phys. Rev. Res. **3**, 023040 (2021).

[39] S.-F. Liou, F. D. M. Haldane, K. Yang, and E. H. Rezayi, Chiral gravitons in fractional quantum Hall liquids, Phys. Rev. Lett. **123**, 146801 (2019).

[40] L. D. Barron, L. Hecht, I. H. McColl, and E. W. Blanch, Raman optical activity comes of age, Mol. Phys. **102**, 731 (2004).

[41] See Supplemental Material at http://link.aps.org/supplemental/10.1103/PhysRevResearch.6.L022005 for more experimental details.

[42] C. Chen, X. Chen, B. Deng, K. Watanabe, T. Taniguchi, S. Huang, and F. Xia, Probing interlayer interaction via chiral phonons in layered honeycomb materials, Phys. Rev. B **103**, 035405 (2021).

[43] T. Zhang and S. Murakami, Chiral phonons and pseudoangular momentum in nonsymmorphic systems, Phys. Rev. Res. **4**, L012024 (2022).

[44] K. Jenni, S. Kunkemöller, W. Schmidt, P. Steffens, A. A. Nugroho, and M. Braden, Chirality of magnetic excitations in ferromagnetic $SrRuO_3$, Phys. Rev. B **105**, L180408 (2022).

[45] J. Cenker, B. Huang, N. Suri, P. Thijssen, A. Miller, T. Song, T. Taniguchi, K. Watanabe, M. A. McGuire, D. Xiao *et al.*, Direct observation of two-dimensional magnons in atomically thin CrI_3, Nat. Phys. **17**, 20 (2021).

[46] R. Hisatomi, A. Noguchi, R. Yamazaki, Y. Nakata, A. Gloppe, Y. Nakamura, and K. Usami, Helicity-changing Brillouin light scattering by magnons in a ferromagnetic crystal, Phys. Rev. Lett. **123**, 207401 (2019).

[47] B. Lyu, Y. Gao, Y. Zhang, L. Wang, X. Wu, Y. Chen, J. Zhang, G. Li, Q. Huang, N. Zhang *et al.*, Probing the ferromagnetism and spin wave gap in VI_3 by helicity-resolved Raman spectroscopy, Nano Lett. **20**, 6024 (2020).

[48] K. R. Hoffman, D. J. Lockwood, and W. M. Yen, Circular dichroism and Raman optical activity in antiferromagnetic transition-metal fluorides, Low Temp. Phys. **31**, 786 (2005).

[49] The features M1, M2, and M3 correspond to $m_{1\alpha}$, $m_{2\gamma}$, and $m_{2\alpha}$ in Ref. [15] and to M1, 2M, and 3M in Ref. [32], while M0 corresponds to MB in Ref. [32]. Note that previous data were reported in the I_{+-} [15] and I_{-+} channels [32]. Due to the pronounced ROA for intermediate fields, not all features are discussed in all previous studies.

[50] We use a base temperature of 1.7 K. Via the suppression of the magnon intensity, we estimate the local sample temperature at the laser spot to be $T_N \sim 7$ K at 40 μW. Comparing Stokes and anti-Stokes scattering, we find temperature ∼25 K at 250 μW and ∼41 K at 1000 μW. See, also, the Supplemental Material [41].

[51] D. G. Joshi, Topological excitations in the ferromagnetic Kitaev-Heisenberg model, Phys. Rev. B **98**, 060405(R) (2018).

[52] P. A. McClarty, X.-Y. Dong, M. Gohlke, J. G. Rau, F. Pollmann, R. Moessner, and K. Penc, Topological magnons in Kitaev magnets at high fields, Phys. Rev. B **98**, 060404(R) (2018).

[53] L. E. Chern, E. Z. Zhang, and Y. B. Kim, Sign structure of thermal Hall conductivity and topological magnons for in-plane field polarized Kitaev magnets, Phys. Rev. Lett. **126**, 147201 (2021).